Friction induced limit cycling : hunting

Friction Induced Limit Cycling: Hunting

R.H.A.Hensen

DCT Internal Report 2001.21

Eindhoven University of Technology
Department of Mechanical Engineering
Dynamics and Control Technology Group

Friction Induced Limit Cycling: Hunting

R.H.A. Hensen [a], M.J.G. van de Molengraft [a], M. Steinbuch [a]

[a] *Control Systems Technology Group, Department of Mechanical Engineering, Eindhoven University of Technology, P.O. Box 513, 5600 MB, Eindhoven, The Netherlands*

Abstract

In this paper friction induced limit cycles are predicted for a simple motion system of a single motor-driven inertia subjected to friction and a PID-controlled regulator task. The two friction models used, i.e., (i) the dynamic LuGre friction model and (ii) the static Switch friction model, are compared with respect to the so-called hunting phenomenon. Analysis tools originating from the field of nonlinear dynamics will be used to investigate the friction induced limit cycles. For a varying controller gain, stable and unstable periodic solutions are computed numerically which, together with the stability analysis of the closed-loop fixed points, result in a bifurcation diagram. For both friction models, the bifurcation analysis indicates the disappearance of the hunting behaviour for controller gains larger than the gain corresponding to the cyclic fold bifurcation point.

Key words: Friction; Limit Cycles; PID control; Stability Analysis.

1 Introduction

Friction is to some extent present in all mechanical systems. In servo or tracking systems friction can severely limit the performance in terms of increasing tracking errors and the occurrence of limit cycles, i.e., periodic solutions of the nonlinear autonomous system. Especially, limit cycling is an undesirable phenomenon in controlled servo systems because of its oscillatory and persistent behavior. Limit cycling is mainly caused by the combination of the difference in static and Coulomb friction and integral action in the control loop. A regulator task might end up in a stick-slip oscillation around the reference position, which is called hunting [1].

To predict and simulate the hunting behaviour in servo systems, an appropriate friction model has to be chosen. Here, the sophisticated LuGre friction model [4] and the Switch friction model [15] are compared with respect to the hunting phenomenon. This comparison will be on a qualitative basis since we are interested in the computationally most convenient and simple friction model without violating the properties of the phenomenon.

Commonly used analysis tools to predict the existence of the hunting limit cycles are: (i) the Describing Function Analysis (DFA), (ii) the Phase Plane Analysis (PPA); for references see [1] and (iii) exact analysis performed both numerically and algebraically.
The DFA for the LuGre friction model is performed in [9] and resulted in a qualitative prediction of the limit cycles. The idea of the DFA is to divide the closed-loop autonomous system in a linear part $y = H(s)x$ with transfer function $H(s) = \frac{Y(s)}{X(s)}$ and a nonlinear part $x = \varphi(y)$. A major drawback of the DFA is the assumption that the input of the nonlinear part x is close to a nonbiased sinusoid, which assumption is often not justified.
A PPA technique is used to compare different friction models with respect to the hunting behaviour in [20]. It states that suitable stick-slip friction models are those which have a damping function that drops for non-zero velocity from the static friction force level, either continuously or discontinuously, to a lower value than the static level. A one-dimensional mapping technique is used to find solely stable periodic solutions. The search for unstable limit cycles and the stability analysis of the equilibrium

Email addresses: R.H.A.Hensen@tue.nl (R.H.A. Hensen), M.J.G.v.d.Molengraft@tue.nl (M.J.G. van de Molengraft), M.Steinbuch@tue.nl (M. Steinbuch).

points are not performed.
An exact analysis of limit cycles caused by friction is performed by [18]. The period and amplitude of the limit cycle, induced by a simplified friction model, are computed numerically by solving nonlinear equations. Conditions for local stability of the periodic solution are obtained and stable solutions are found for various controller settings.
An exact algebraic analysis is compared to the DFA for a PID controlled system in the presence of static friction in [2]. The paper states that for Coulomb friction combined with a larger static friction the controlled system will lead to a friction induced limit cycle for all stabilizing controllers. The authors conclude that their result is inadequate to practically observed behaviour where hand-tuned PID controllers indeed eliminate stick-slip oscillations. Hence, the use of a more complete dynamic friction model is advised by [2] and that will be the focus here.

To obtain a qualitatively and quantitatively good prediction of limit cycles generated by more general friction models, like the dynamic LuGre and static Switch friction model, we will use analysis tools originating from nonlinear dynamics, i.e., bifurcation theory, shooting methods and path-following techniques [11]. Limit cycles, that are searched for with shooting methods [15], will be tested for stability by means of the *Floquet multipliers* [11]. Branches of stable and unstable periodic solutions, found by path-following techniques [8], result in a bifurcation diagram. The advantage of this approach is that even for sophisticated friction models exact predictions of the limit cycles are obtained and information on the local stability is provided. Furthermore, the possible disappearance of the limit cycle for certain controller settings is illustrated in the bifurcation diagram.

The outline of this paper is as follows. In Section 2, we will give a description of the hunting phenomenon. A qualitative comparison with respect to hunting between the LuGre model and the Switch model will be given in Section 3. The numerical methods used to compute the bifurcation diagram and the stability test performed will be discussed in Section 4. The bifurcation diagram in terms of the controller gain K for the two nonlinear autonomous systems will be obtained by means of path-following techniques in Section 5. In Section 6 the paper will be concluded and future research topics will be addressed.

2 Hunting

Consider a simple motion system consisting of a single motor-driven inertia subjected to friction:

$$J\ddot{\theta} = -F + c_m u$$

where F is the friction torque, c_m the motor constant and u the input motor torque. For a regulator task, the desired angle θ_d is constant in time. The use of a PD controller would lead to a steady state error due to the presence of friction. Therefore, a PID-type controller will be used here.

Here, a fixed controller structure $C(s)$ is used composed of a lead-lag controller $C_{ll}(s)$ and integral controller part $C_i(s)$

$$C(s) = C_{ll}(s)C_i(s) = K(\tau_d s + 1)(\frac{\tau_i s + 1}{\tau_i s})$$

where only the controller gain K can be altered. The controller shape, determined by $\tau_i = \frac{1}{2\pi f_i}$ and $\tau_d = \frac{1}{2\pi f_d}$, is fixed with $f_i = f_d = 1$ [Hz] and is shown in Figure 1 for $K = \{0.04, 0.1\}$.

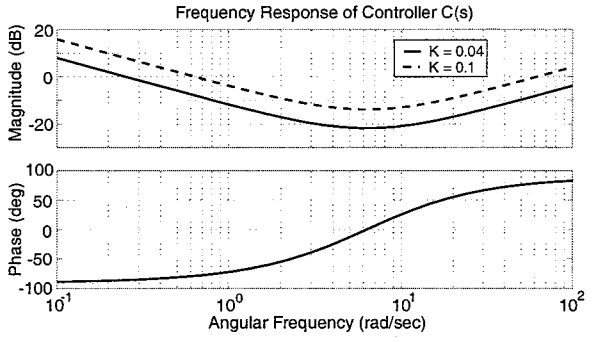

Figure 1. Fixed controller shape.

In the time-domain this controller turns into

$$u = K[(1 + \frac{\tau_d}{\tau_i})(\theta_d - \theta) - \tau_d\dot{\theta} + \frac{1}{\tau_i}\int_0^t (\theta_d - \theta(\tau))d\tau]$$

and the closed-loop system becomes

$$J\ddot{\theta} - c_m K[(1 + \frac{\tau_d}{\tau_i})(\theta_d - \theta) - \tau_d\dot{\theta} + \frac{1}{\tau_i}\int_0^t (\theta_d - \theta(\tau))d\tau] = -F$$

For the linear system without friction a stability condition for the closed-loop system can be obtained by the Routh-Hurwitz criterion that results in $K > \frac{J}{c_m \tau_d(\tau_d+\tau_i)}$. We assume that this lower bound is also applicable to the non-linear system, since the friction force will dissipate energy from the system. In the sequel of this paper the fixed controller shape will be utilized, i.e., $\tau_i = \tau_d = \frac{1}{2\pi}$.

In an experimental setup as described in [13], this controller is used to perform a regulator task with $\theta_d = 1$ [rad] and $K = 0.04$. In Figure 2, the angular displacement θ, angular velocity $\dot{\theta}$, integral term $\int_0^t(\theta - \theta_d)dt$ and the control effort u are depicted. The response of the system enters a hunting behavior and will not reach the desired angular position. The phenomenon can be characterized in various ways and one way is to determine the amplitude and frequency of the periodic motion. Due to direction-dependent, position-dependent and time-varying friction behaviour, the limit cycle is not symmetric and its frequency not constant in time. Hence, the amplitude and frequency are obtained by averaging the properties over consecutive periods. For this closed-loop system the hunting response can be described by an average amplitude of $|\theta - \theta_d| = 0.061$ [rad] and an average frequency of $f = 0.122$ [Hz].

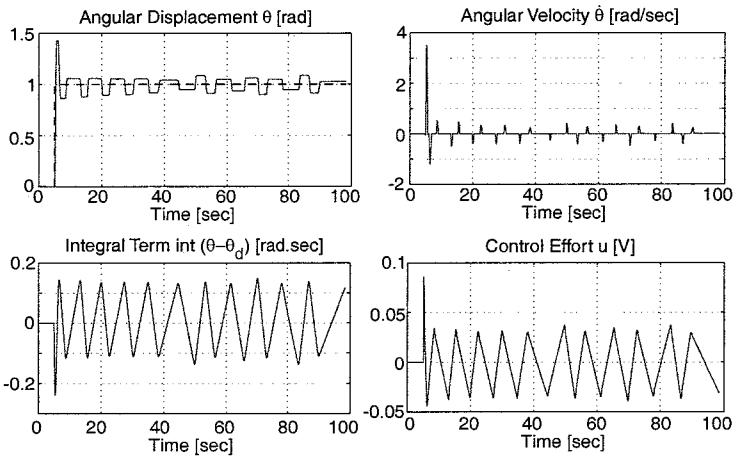

Figure 2. Hunting limit cycling.

3 Friction Model Comparison with respect to Hunting

In this section two friction models, i.e., the LuGre model and the Switch model, will be discussed in terms of the resulting closed-loop autonomous system and the hunting behaviour.

3.1 The dynamic LuGre friction model

In the past decade, the interest in dynamic friction models increased [4], [3], [12] resulting in a number of dynamic friction models based on the Dahl model [7]. The LuGre model is such a dynamic friction model and exhibits a rich behaviour of friction phenomena, e.g., presliding displacement, frictional lag and varying break-away force, which have all been observed

in practice. Hence, the LuGre model will be used to predict and simulate hunting limit cycles. The friction force is described as

$$F = \sigma_0 z + \sigma_1 \frac{dz}{dt} + \sigma_2 \dot{\theta}$$
$$\frac{dz}{dt} = \dot{\theta} - \frac{|\dot{\theta}|}{g(\dot{\theta})} z$$

where z is an extra state representing the average microscopic deflection of the so-called bristles located between the two sliding surfaces [12], $\dot{\theta}$ the relative velocity between the moving parts, $g(\dot{\theta})$ the Stribeck curve, σ_0 the stiffness of the bristles, σ_1 the damping of the bristles and σ_2 the viscous friction coefficient. For ease throughout the paper, the states of the closed-loop system are redefined as

$$x_1 = (\theta - \theta_d)$$
$$x_2 = \dot{\theta}$$
$$x_3 = \int_0^t (\theta(\tau) - \theta_d) d\tau = \int_0^t x_1 d\tau$$
$$x_4 = z$$

The autonomous system can be written as a set of continuous non-smooth stiff differential equations, i.e.,

$$\dot{\underline{x}} = f_{LuGre}(\underline{x}) = \begin{cases} x_2 \\ -\frac{2Kc_m}{J} x_1 - (\frac{Kc_m}{2\pi J} + \frac{\sigma_2 + \sigma_1}{J}) x_2 - \frac{2\pi Kc_m}{J} x_3 - \frac{\sigma_0}{J} x_4 + \frac{\sigma_1 \sigma_0}{J} \frac{|x_2|}{g(x_2)} x_4 \\ x_1 \\ x_2 - \sigma_0 \frac{|x_2|}{g(x_2)} x_4 \end{cases}$$

where $\underline{x} = [x_1 \; x_2 \; x_3 \; x_4]^T$.

3.2 The static Switch friction model

In contrast to the dynamic friction model mentioned above, the Switch model [15] is a static friction model that can be considered as a modified version of the Karnopp model [14]. The Switch model distinguishes three situations: (i) the slip phase, (ii) the stick phase and (iii) the transition phase. The latter describes the transition from stick to slip or velocity reversals without stiction. As for the Karnopp friction model, the different phases are described by ordinary differential equations (ODEs) and a narrow band around zero velocity is introduced. In this narrow band, the system can be in the stick phase or in the transition phase as illustrated in Figure 3. In this figure the narrow stick band is shown together with possible vectorfields belonging to the three phases. The friction force is given by

$$F(x_2, u) = \begin{cases} g(x_2)\text{sgn}(x_2), & \forall \; |x_2| > \eta \\ F_s \text{sgn}(u), & \forall \; |x_2| \leq \eta \text{ and } |u| > F_s \\ u - \alpha x_2, & \forall \; |x_2| \leq \eta \text{ and } |u| \leq F_s \end{cases}$$

where u is the applied control effort, F_s is the static friction, η represents the narrow stick band around $x_2 = 0$ with $\eta \ll 1$ and $g(x_2)$ is again the Stribeck curve as described for the LuGre friction model. The closed-loop state equations for the Switch

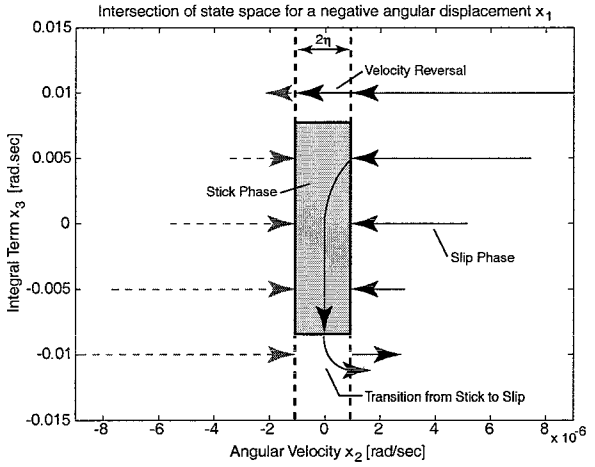

Figure 3. Intersection of state space for a negative angular displacement x_1.

model read

$$\dot{\underline{x}} = f_{Switch}(\underline{x})$$

$$= \begin{cases} \begin{bmatrix} x_2 \\ -\frac{2Kc_m}{J}x_1 - (\frac{Kc_m}{2\pi J} + \frac{\sigma_2}{J})x_2 - \frac{K2\pi c_m}{J}x_3 - \frac{g(x_2)}{J}\mathrm{sgn}(x_2) \\ x_1 \end{bmatrix} & \forall\, |x_2| > \eta \\ \begin{bmatrix} x_2 \\ -\frac{2Kc_m}{J}x_1 - (\frac{Kc_m}{2\pi J} + \frac{\sigma_2}{J})x_2 - \frac{K2\pi c_m}{J}x_3 - \frac{F_s}{J}\mathrm{sgn}(u) \\ x_1 \end{bmatrix} & \forall\, |x_2| \leq \eta \text{ and } |u| > F_s \\ \begin{bmatrix} 0 \\ -\alpha x_2 \\ x_1 \end{bmatrix} & \forall\, |x_2| \leq \eta \text{ and } |u| \leq F_s \end{cases}$$

where the applied control effort $u = 2Kc_m x_1 + \frac{Kc_m}{2\pi}x_2 + K2\pi c_m x_3$ and the acceleration term $-\alpha x_2$ in the stick phase forces the velocity x_2 to zero for $\alpha > 0$. This acceleration term ensures that the ODE belonging to the stick phase does not suffer from numerical instabilities as in the Karnopp friction model. In this paper the Switch model will be regarded as a Discrete Event System. Hence, the time instances at which the system switches from one phase to another are detected exactly and the ordinary differential equation corresponding the next phase is used to proceed.

3.3 Parameter identification

The identification of the friction models is not the subject of this paper. However, it is very important to identify the various friction parameters accurately to obtain good quantitative predictions. The friction models have been identified with an odd Stribeck curve $g(x_2)$ to simplify both the estimation and analysis of the closed-loop systems. The Stribeck curve describes a continuous drop from the static friction level F_s to a lower Coulomb friction level F_c. This decrease in friction is necessary to obtain limit cycles as shown in [20], [2] and can be modeled as

$$g(x_2) = F_c + (F_s - F_c)\exp^{-(\frac{x_2}{v_s})^2}$$

where v_s is the so-called Stribeck velocity, which determines the speed of decrease for the friction curve. The identification of the LuGre model has been performed as described in [5] and the estimated Stribeck curve is also used in the Switch model.

3.4 *Comparison of the hunting behaviour*

To compare both models in terms of the hunting behaviour, the same regulator task $\theta_d = 1$ [rad] as for the experimental setup in Section 2 is considered. The closed-loop responses for both models end up in a hunting limit cycle. Contrary to the time-varying hunting behaviour of the experimental setup the predicted limit cycles are symmetric and the closed-loop dynamics is time-invariant. Hence, a good comparison with experimental data is difficult, but one period of the response in Figure 2, i.e., from ± 75 [sec] to ± 85 [sec], is approximately symmetric. In Figure 4, this period of the limit cycle (-) is compared

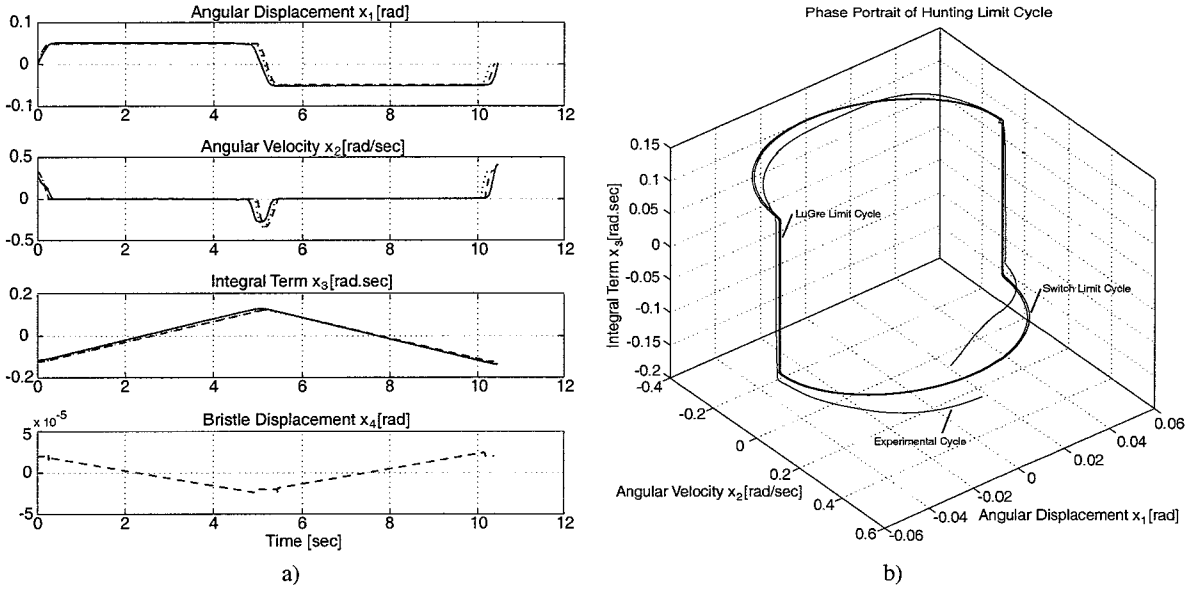

Figure 4. Hunting limit cycle.

with (i) the LuGre system (- -) and (ii) the Switch system (:). The time responses of the system states are shown in Figure 4 (a) and their phase portraits of the first three states are depicted in Figure 4 (b). The experimentally observed cycle can be predicted with reasonable accuracy by both models whereas the difference between the two predicted cycles is negligible. The sophisticated LuGre adds no extra frictional behaviour essential to the hunting phenomenon. The LuGre system has an extra state in comparison with the Switch system and the stiffness of the LuGre system is considerably larger. On the other hand, the treatment of a Discrete Event System introduces additional computational effort for the Switch system. To evaluate the Switch model, the integration process is halted on the transition between the slip and stick phase of the system (and visa versa), the discontinuity is found by an iterative process and the integration is restarted. Furthermore, the investigation on the change of system characteristics (bifurcation diagram) might be influenced by the choice of a discontinuous model such as the Switch model. A discontinuous system can introduce discontinuous bifurcations [16], which can never occur for the continuous LuGre model. Hence, in the following section the determination of the bifurcation diagram will be performed for both models.

4 Bifurcation Diagram

The bifurcation diagram is obtained by using analysis tools originating from the field of nonlinear dynamics. Fixed points or equilibria are tested on local stability and periodic solutions are sought with a shooting method. The local stability of the limit cycles is investigated by examining its *Floquet multipliers*. For varying controller gain K, periodic solutions are found with path-following techniques resulting in a bifurcation diagram.

4.1 *Fixed points and local stability*

The equilibrium points or fixed points of autonomous systems satisfy the condition

$$f(\underline{x}) = 0$$

and the local stability of these fixed points is determined by the eigenvalues of the Jacobian matrix. First of all, it is important to realize that the equilibrium points of interest are those for which the position error x_1 and velocity error x_2 are zero. The integral term x_3 for either model and, additionally for the LuGre model, the bristle deflection x_4 should not necessarily be zero, since it involves a regulator task.

The fixed points of interest for the LuGre system are located on a hyperplane spanned by

$$\underline{x}^*_{LuGre} = \alpha \begin{bmatrix} 0 \\ 0 \\ -\frac{\sigma_0}{K2\pi c_m} \\ 1 \end{bmatrix},$$

where $|\alpha| \leq \frac{F_s}{\sigma_0}$ if the initial state $|x_4(0)| \leq \frac{F_s}{\sigma_0}$ [4]. This invariant set means that the force produced from a non-zero bristle deflection is compensated by the integral action. Hence, one eigenvalue of the Jacobian matrix in $\underline{x}^*_{LuGre}$ should be zero with an eigenvector equal to $[0 \;\; 0 \;\; -\frac{\sigma_0}{K2\pi c_m} \;\; 1]^T$. Due to the non-smoothness of the LuGre model, i.e., the absolute function $|x_2|$ in the differential equations, the derivation of this Jacobian matrix needs special attention. The notion of *generalized differentials* [6] is essential and states that the *generalized derivative* of f at x is declared as *any* value $f'_q(x)$ included between its left and right derivatives. The closed convex hull of the derivative extremes is called the *generalized differential* of f at x.

$$\begin{aligned} \partial f &= \overline{\text{co}}\{f'_-, f'_+\} \\ &= \{f'_q(x) | f'_q(x) = (1-q)f'_- + qf'_+, \quad \forall q \mid 0 \leq q \leq 1\} \end{aligned}$$

Now, the generalized differential of the vector field $f_{LuGre}(\underline{x})$ with respect to $\underline{x}$ can be regarded as the generalized Jacobian $\tilde{J}$:

$$\tilde{J} = \partial_{\underline{x}} f_{LuGre} = (1-q)J_- + qJ_+, \quad 0 \leq q \leq 1$$

where J_- and J_+ are respectively the Jacobian matrices from below and above $x_2^* = 0$. The generalized Jacobian in $\underline{x}^*_{LuGre}$ is

$$\tilde{J}_q(\underline{x}^*_{LuGre}) = \begin{bmatrix} 0 & 1 & 0 & 0 \\ -\frac{2Kc_m}{J} & -(\frac{Kc_m}{2\pi J} + \frac{\sigma_2+\sigma_1}{J}) + \frac{\sigma_1\sigma_0\alpha(2q-1)}{JF_s} & -\frac{K2\pi c_m}{J} & -\frac{\sigma_0}{J} \\ 1 & 0 & 0 & 0 \\ 0 & 1 - \frac{\sigma_0\alpha(2q-1)}{F_s} & 0 & 0 \end{bmatrix} \quad \forall \quad 0 \leq q \leq 1, \quad |\alpha| \leq \frac{F_s}{\sigma_0}.$$

The three non-zero eigenvalues have to be in the open left-half plane for all $0 \leq q \leq 1$ and $|\alpha| \leq \frac{F_s}{\sigma_0}$ to guarantee the local stability of the fixed points. Hence, the characteristic equation

$$\det(\tilde{J}_q(\underline{x}^*_{LuGre}) - \lambda I) = 0$$

belonging to this eigenvalue problem has one eigenvalue equal to zero and the remaining polynomial should have

- coefficients larger than zero, which results in the condition that all system parameters, including the controller gain K, should be positive and
- a sufficient condition can be constructed from the Routh-Hurwitz criterion as follows:

$$\begin{aligned} (\frac{Kc_m}{2\pi J} + \frac{\sigma_2+\sigma_1}{J}) &> \frac{K2\pi c_m}{\sigma_0(1 - \frac{\sigma_0\alpha(2q-1)}{F_s}) + 2Kc_m} + \frac{\sigma_1\sigma_0\alpha(2q-1)}{JF_s} \quad \forall \quad 0 \leq q \leq 1, \quad |\alpha| \leq \frac{F_s}{\sigma_0} \\ &> \pi + \frac{\sigma_1}{J}. \end{aligned}$$

which together with the first condition results in

$$\frac{\sigma_2}{J} > \pi$$

The fixed points of interest for the autonomous system concerning the Switch model are located on the line

$$\underline{x}^*_{Switch} = \beta \begin{bmatrix} 0 \\ 0 \\ 1 \end{bmatrix}, \quad \forall\, |\beta| < \frac{F_s}{Kc_m 2\pi}.$$

Again an invariant direction where the applied control effort $u = Kc_m 2\pi x_3^*$ is compensated by an equivalent portion of the static friction F_s and results in exactly the same equilibrium points as for the first three states of the LuGre closed-loop system. The local stability of such an invariant set is not trivial. The idea used here is that in the vicinity of the equilibrium points there should be a region for which all solutions, starting within this region, stay within this domain and finally end up in the stick phase, i.e., $|x_2| \leq \eta$ and $|x_1 + \pi x_3| \leq \frac{F_s}{2Kc_m}$. First, the convergence to the stick phase is investigated and a bound on the states is obtained. For the slip phase, i.e., $|x_2| > \eta$, the equation of motion can be written as:

$$\dot{x}_2 + (\frac{Kc_m}{2\pi J} + \frac{\sigma_2}{J})x_2 + \frac{g(x_2)}{J}\text{sgn}(x_2) = -\frac{2Kc_m}{J}x_1 - \frac{K2\pi c_m}{J}x_3 \tag{1}$$

which has a similar structure as the equations generally derived in sliding controllers, i.e., $\dot{x}_i + h_i \text{sgn}(x_i) = 0$. For this kind of systems it can be shown that for positive $h_i\ \forall\ x_i$ the state x_i converges to zero. To obtain this form, the righthand side of Eq. (1) should be bounded by $|\frac{2Kc_m}{J}x_1 + \frac{K2\pi c_m}{J}x_3| < \frac{g(x_2)}{J}$. Namely, in this case the righthand side of Eq. (1) can be written as:

$$\frac{2Kc_m}{J}x_1 + \frac{K2\pi c_m}{J}x_3 = \alpha(x_2)\text{sgn}(x_2) \quad \text{for } |x_2| > \eta \tag{2}$$

with $-\frac{g(x_2)}{J} < \alpha(x_2) < \frac{g(x_2)}{J}$. Substitution of (2) in (1) gives

$$\dot{x}_2 + (\frac{Kc_m}{2\pi J} + \frac{\sigma_2}{J})x_2 + (\frac{g(x_2)}{J} + \alpha(x_2))\text{sgn}(x_2) = 0, \tag{3}$$

with $0 < (\frac{g(x_2)}{J} + \alpha(x_2)) = \beta(x_2) < 2\frac{g(x_2)}{J}$, i.e., $\beta(x_2)$ represents a positive-valued variable for $g(x_2) > 0 \quad \forall x_2$ and $J > 0$. Hence, stability can be shown with the candidate Lyapunov function

$$V(x_2) = \frac{1}{2}x_2^2,$$

and its derivative

$$\begin{aligned} \dot{V}(x_2) &= x_2\dot{x}_2 \\ &= -\beta(x_2)x_2\text{sgn}(x_2) - (\frac{Kc_m}{2\pi J} + \frac{\sigma_2}{J})x_2^2 \\ &= -\beta(x_2)|x_2| - (\frac{Kc_m}{2\pi J} + \frac{\sigma_2}{J})x_2^2 \\ &< 0, \quad \forall x_2 \neq 0, \quad (\frac{Kc_m}{2\pi J} + \frac{\sigma_2}{J}) > 0. \end{aligned}$$

Within the bound $|\frac{2Kc_m}{J}x_1 + \frac{K2\pi c_m}{J}x_3| < \frac{g(x_2)}{J}$, convergence to the stick phase $|x_2| \leq \eta$ is guaranteed. In Figure 5, an example of this bound on the states is depicted for various angular displacements x_1. The actual region of attraction to the stick phase is determined by those solutions which, initialized within the obtained bound, stay within this bound for all time. Due to the nonlinear frictional Stribeck curve algebraic solutions of the motion in slip phase are not derivable and the actual attraction regime can not be computed. Numerical investigation of this problem is even more complicated, since infinite many initial conditions should be evaluated, which will not be performed here. However, if there exists such a region of attraction and the system enters the stick phase, the position error x_1 should be in the regime of attraction of the fixed points which is determined by the bifurcation diagram.

For both models, the desired position of the regulator task is a fixed point of the autonomous system. In the sequel, the local stability condition for the LuGre equilibrium points will be checked and the local stability of the invariant set for the Switch model will be investigated by examination of the bifurcation diagram.

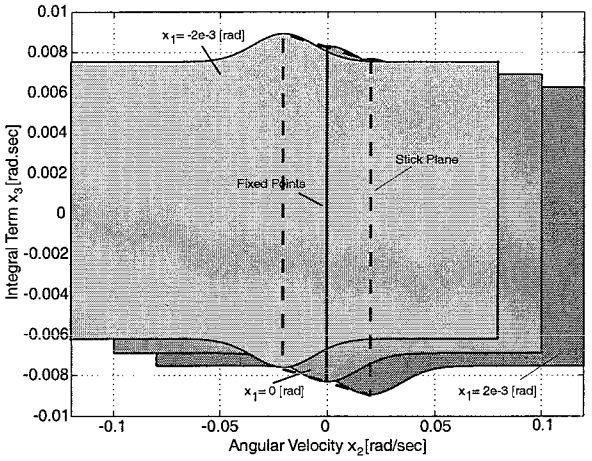

Figure 5. Bounds on the states for various angular displacements x_1.

4.2 Periodic solutions and Floquet multipliers

Hunting limit cycles, as given in Figures 4 (a-b), can be regarded as a fixed point of a Poincaré map P on a Poincaré section. For the Switch closed-loop system, a Poincaré section might be the plane $x_1 = 0$ in Figure 4 (b). The stability of a periodic solution is determined by its *Floquet multipliers* λ_i $(i = 1, \ldots, n)$, which are the eigenvalues of the fundamental solution matrix $\underline{\Phi}(T + t_0, t_0)$ [11], where T is the period time of the solution. For local stability analysis of periodic solutions, the Floquet multipliers are the generalization of the eigenvalues at a fixed point. For the autonomous systems considered here, a perturbation along the solution will give the same, however time-shifted, periodic solution. This means that one of the Floquet multipliers equals unity. The periodic solution is stable if all Floquet multipliers, that are not associated with the phase, lie within the unit circle. If one or more Floquet multipliers lie outside the unit circle, then the periodic solution is unstable. The periodic solution, as well as its Floquet multipliers, changes as a parameter of the closed-loop system, e.g., the controller gain K, is altered. The limit cycle changes from stable to unstable or vise versa when the largest Floquet multiplier passes through the unit circle.

For smooth systems, the fundamental solution matrix $\underline{\Phi}(T+t_0, t_0)$, which is also known as the monodromy matrix $\underline{\Phi}_T$ after one period time T, can be computed by solving the *variational equation* [19]. However, the models used are non-smooth and the *variational equation* is not applicable as demonstrated by [15], [16]. Here, the monodromy matrix is obtained by a sensitivity analysis [15], where an initial state vector $\underline{x}_0$ is perturbed component-wise and the system is integrated over the period time T. The differences between the unperturbed final state vector $\underline{x}_T$ and the perturbed final state vectors $\underline{x}_T^j$ $(j = 1, \ldots, n)$ are used to compute the elements of the monodromy matrix.

To find either stable or unstable periodic solutions for the non-smooth autonomous systems as described in Section 3, the monodromy matrix obtained by the sensitivity analysis is used in a (single) shooting method [19]. The advantage of this two-point boundary value problem (BVP) solver is the ability to find unstable periodic solutions. Furthermore, the shooting method is used in a path-following algorithm [8] to investigate the influence of a parameter of the closed-loop system on the periodic solution. Here, the algorithm calculates a branch of periodic solutions for the varying controller gain K and a so-called bifurcation diagram is obtained.

5 Numerical Results

The system parameters used to perform the stability test for the fixed points and to obtain stable and unstable branches of periodic solutions are given in Table 1. The controller gain K is the closed-loop system parameter to be changed and the Routh-Hurwitz stability criterion as described in Section 2, i.e., $K > \frac{J}{c_m \tau_d (\tau_d + \tau_i)} = 0.0321$ will be used as a lower bound. The hunting limit cycles will be characterized with the maximal angular displacement, i.e., $\max |x_1(t)| \; \forall \; 0 \leq t \leq T$, and the period time T. Stable branches are depicted with solid lines (-) and unstable branches with dashed lines (- -).

5.1 The bifurcation diagram for the LuGre system

For the LuGre closed-loop system it is possible to check the local stability conditions for the fixed points as described in Section 4.1. The system parameters, as given in Table 1, together with the Routh-Hurwitz lower bound on K are all positive, so the first condition is satisfied. Since the second condition

$$\frac{\sigma_2}{J} = 3.8461538 > \pi$$

is also satisfied, the fixed points are locally stable and the branch $x_1 = 0$ is stable as shown in Figure 6 (a). In this figure

Inertia	$J = 0.026$ [kg.m^2]
Motor Gain	$c_m = 16$ [N.m/V]
Static Friction	$F_s = 0.53$ [N.m]
Coulomb Friction	$F_c = 0.44$ [N.m]
Stribeck Velocity	$v_s = 0.02$ [rad/s]
Viscous Damping	$\sigma_2 = 0.1$ [N.m.s/rad]
Stick Band	$\eta =$ 1e-6 [rad/s]
Time Constant	$\alpha = 10$ [1/s]
LuGre Bristle Stiffness	$\sigma_0 =$ 2.2e+4 [N.m/rad]
LuGre Bristle Damping	$\sigma_1 = 7.58$ [N.m.s/rad]

Table 1
Closed-loop system parameters.

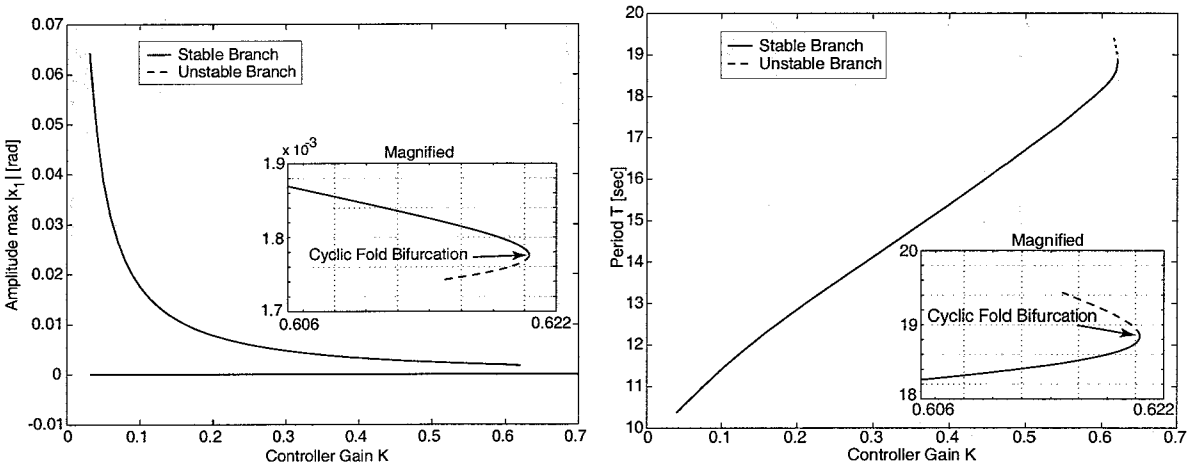

a) Amplitude versus controller gain K

b) Period time versus controller gain K

Figure 6. Bifurcation diagram for the LuGre closed-loop system.

both the amplitude and period time of the periodic solutions are depicted. The path-following is started on the stable branch for $K = 0.0321$ and terminated on the unstable branch at $K = 0.615$. The algorithm is halted due to the extensive computational effort needed to follow the path and the fact that we are mainly interested in the bifurcation point that is given by the intersection of the stable and unstable branch at $K = 0.620$. However, investigation of the bifurcation diagram, as given in Figure 6 (a), shows locally stable fixed points together with locally stable periodic solutions for controller gains smaller than the bifurcation point and an unstable branch might be expected in between.

Figure 7 show the Floquet multipliers $\lambda_i, \quad i = 1, \ldots, 4$, where all multipliers are on the real axis. Floquet multiplier λ_1 is equal to one due to the phase of the limit cycles. Two multipliers are close to zero and one multiplier λ_2 varies as the controller gain K changes. The Floquet multiplier λ_2 predicts a bifurcation point since it passes the value +1 at $K = 0.620$. Hence,

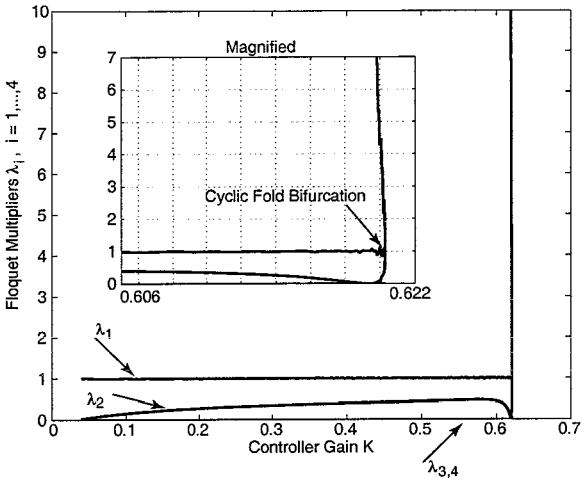

Figure 7. Floquet multipliers for the LuGre closed-loop system.

this bifurcation point is a so-called cyclic fold bifurcation point [8]. Furthermore the bifurcation point is continuous since the Floquet multiplier does not jump through the unit circle [17].

The fixed points, stable and unstable limit cycles for the LuGre system with a controller gain $K = 0.615$ are shown in Figure 8. Only the first three states are plotted to visualize the cycles and to compare the behaviour with the cycles obtained for the

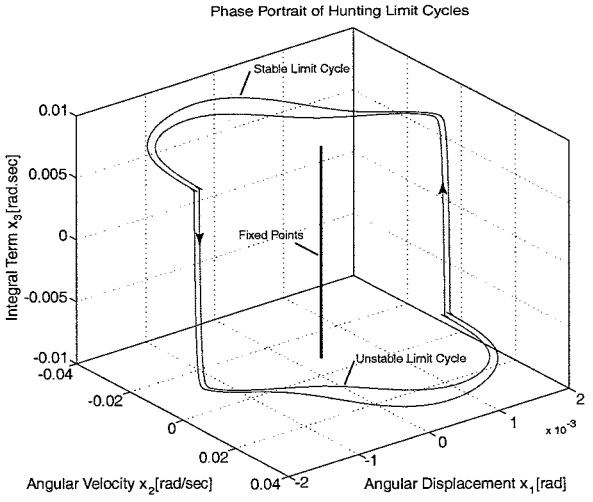

Figure 8. Stable and unstable limit cycles for the LuGre closed-loop system and $K = 0.615$.

Switch system in the next section.

5.2 The bifurcation diagram for the Switch system

Secondly, the bifurcation diagrams for the Switch closed-loop system are constructed. In Figure 9, the stable and unstable branches are shown for both the amplitude and the period time of the periodic solutions. The path-following algorithm is again started on the stable branch at $K = 0.0321$ and terminated on the unstable branch at $K = 0.634$. The algorithm is halted due to the same reasons as given for the LuGre closed-loop system. However, for $K = \{0.0321, 0.2, 0.4, 0.6\}$ the unstable periodic solutions are computed with a single shooting method and depicted by a circle.

The autonomous system is of order $n = 3$ and therefore the number of Floquet multipliers is 3 where one should be equal to unity corresponding the phase shift. The Floquet multipliers, which are all elements of the real axis, are depicted in Figure 10,

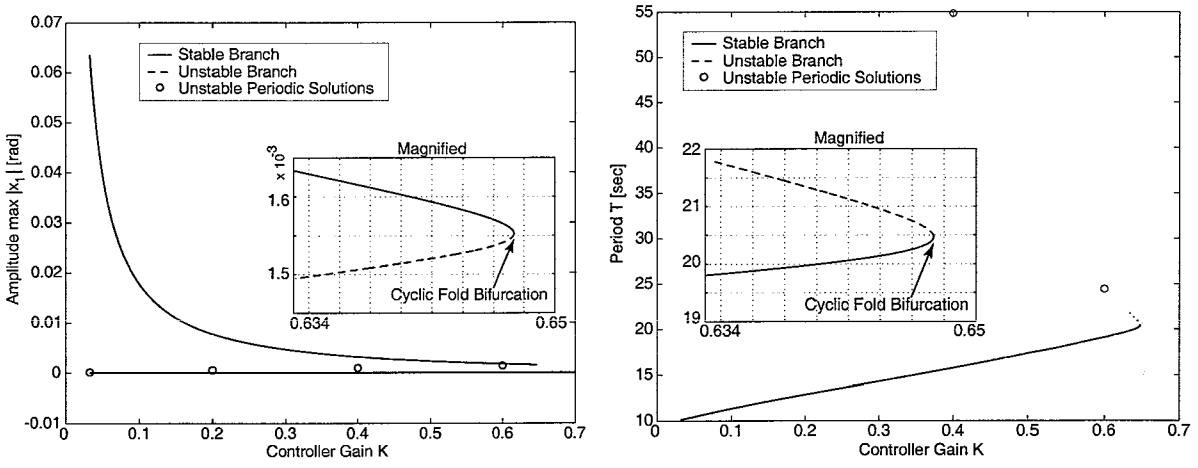

a) Amplitude versus controller gain K

b) Period time versus controller gain K

Figure 9. Bifurcation diagram for the Switch closed-loop system.

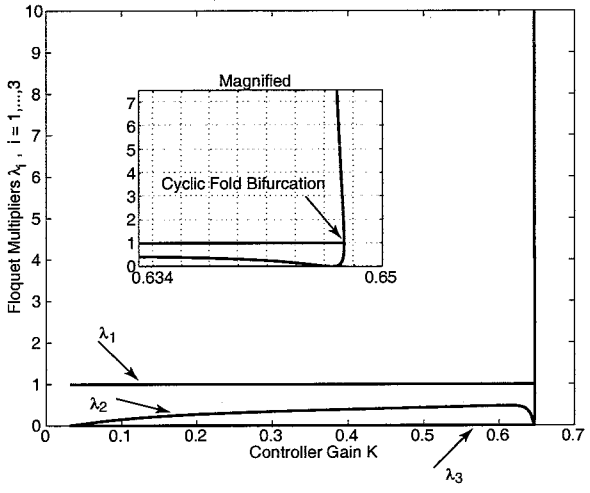

Figure 10. Floquet multipliers for the Switch closed-loop system.

where indeed one Floquet multiplier λ_1 is equal to unity. One multiplier λ_3 is equal to zero and λ_2 varies as the gain is altered and passes through the value +1 for $K = 0.647$, which again detects a cyclic fold continuous bifurcation.

The fixed points, stable and unstable limit cycles for $K = 0.634$ are depicted in Figure 11. The region of attraction of the fixed points in x_1-direction is bounded by the amplitude of the unstable periodic solution, i.e., all trajectories starting in the stick plane and $|x_1| < \max |x_1^{unstable}(t)|$ will end up in an equilibrium point. Hence, the branch $x_1 = 0$ in the bifurcation diagram of Figure 9 (a) is locally stable for perturbations in x_1-direction. It should be emphasized that the stick plane is implemented as a stick volume where in x_2-direction the narrow volume is $2\eta = 2\text{e}{-6}$ [rad/s] thick.

5.3 Remarks on the closed-loop systems

For both systems the nonlinear dynamics are totally described by the second Floquet multiplier in the vicinity of the periodic solutions. For the Switch system, this is due to the fact that state perturbations $\underline{x}(t) + \delta\underline{x}$ in the slip phase reduce in the stick phase to a x_1, x_3 perturbation and *not* in x_2-direction. Furthermore, the perturbation in x_3-direction turns into a phase shift and is therefore not interesting for the dynamics. Moreover, this is not only locally valid around the periodic solutions but for all trajectories that enter the stick phase. Hence, the complex dynamics of this three-dimensional, autonomous, discontinuous Switch system might be described by means of an equivalent one-dimensional map as demonstrated in [20], [10]. [20] shows

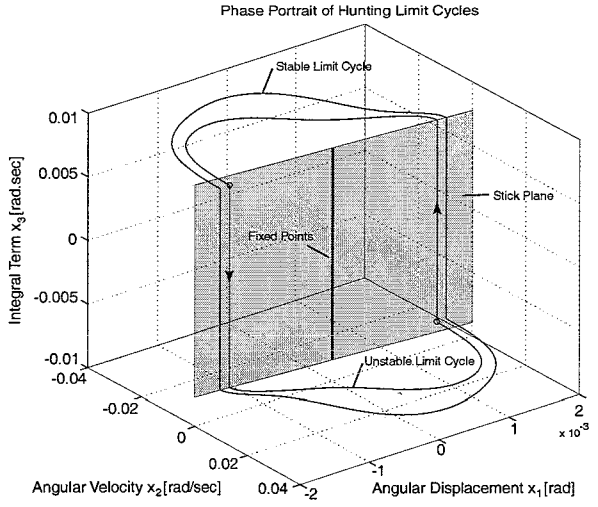

Figure 11. Stable and unstable limit cycles for the Switch closed-loop system and $K = 0.634$.

that this Phase Plane Analysis (PPA) is able to find stable limit cycles, however did not search for unstable limit cycles that should also be able to be constructed with this technique. A two degree-of-freedom stick-slip system is used in [10] to demonstrate the ability to construct such an equivalent one-dimensional event map for a fourth order, autonomous, non-smooth system.

The path-following techniques, used in the previous sections, has been halted on the unstable branch due to the computationally expensive shooting method for unstable systems. For the Switch system, the unstable branch is extended by searching intermediate unstable periodic solutions, since only good initial estimates on the state x_1 and period time T are needed. This is more difficult for the LuGre system due to the necessary good estimates on the entire state (dimension 4) and period time.

6 Conclusions and Future Research

The numerical analysis of the friction induced limit cycles presented in this paper shows the disappearance of the limit cycles for certain system parameters. The tools used enable us to follow branches of stable and unstable periodic solutions. Together with the stability analysis of the equilibrium points, bifurcation diagrams are constructed for both the static Switch friction model and the dynamic LuGre friction model. The resulting diagrams are both qualitatively and quantitatively very much alike, where for both systems cyclic fold continuous bifurcation points are found for a varying controller gain. The location of the bifurcation point is almost the same and the underlying dynamics of the two systems are comparable, since the Floquet multipliers $\lambda_2^{Switch}, \lambda_2^{LuGre}$ for the periodic solutions, describing the closed-loop dynamics, show equivalent behaviour as a function of the control parameter K (compare Figure 7 and 10). Furthermore, the differences of the limit cycles between the LuGre system and the Switch system, as depicted in Figures 4 (b), 8, 11, are small and the cycles are qualitatively the same. Hence, the use of the more sophisticated dynamic LuGre friction model over the static Switch friction model seems not necessary to describe the hunting behaviour properly. The Switch system with its lower order is favorable from a computational point of view and is more easy to visualize and interpret. Moreover, the computational effort to solve the stiff non-smooth continuous LuGre system is more demanding than the effort needed to solve the Discrete Event discontinuous Switch system.

Future research will focus on event mapping techniques to describe the three-dimensional, autonomous, non-smooth Switch system with a one-dimensional map. The event maps can be used to construct a bifurcation diagram such as demonstrated in this paper with shooting and path-following methods. An extension will be to follow the bifurcation point by varying more than one system parameter.

Acknowledgement

The authors are grateful to Dr. Ir. Remco Leine for his contribution to this work.

References

[1] Armstrong-Hélouvry, B., Dupont, P., & Canudas de Wit, C. (1994). A survey of models, analysis tools and compensation methods for the control of machines with friction. *Automatica 30*, 1083-1138.

[2] Armstrong-Hélouvry, B., & Amin, B. (1996). PID Control in the Presence of Static Friction: A Comparison of Algebraic and Describing Function Analysis. *Automatica 32*, 679-692.

[3] Bliman, P.-A., & Sorine, M. (1995). Easy-to-use realistic dry friction models for automatic control. In *Proc. of 3rd European Control Conference.*, Rome, Italy, 3788-3794.

[4] Canudas de Wit, C., Olsson, H., Åström, K.J., & Lischinsky, P. (1995). A New Model for Control of Systems with Friction. *IEEE Transactions on Automatic Control 40*, 419-425.

[5] Canudas de Wit, C., & Lischinsky, P. (1997). Adaptive friction compensation with partially known dynamic friction model. *Int. Journal of Adaptive Control and Signal Processing 11*, 65-80.

[6] Clarke, F.H., Ledyaev, Yu. S., Stern, R.J., & Wolenski, P.R. (1998). Nonsmooth Analysis and Control Theory. *Graduate Texts in Mathematics*, New York.

[7] Dahl, P. (1968). A solid friction model. Aerospace Corp., El Segundo, CA, Tech. Rep. TOR-0158(3107-18)-1.

[8] Fey, R.H.B. (1992). Steady-state behaviour of reduced dynamic systems with local nonlinearities. Ph.D.. Thesis, Eindhoven University of Technology, The Netherlands.

[9] Gäfvert, M. (1997). Comparisons of Two Dynamic Friction Models. *Proc. of the 6th IEEE Conference on Control Applications*, Hartford.

[10] Galvanetto, U., & Knudsen, C. (1997). Event Maps in a Stick-Slip System. *Nonlinear Dynamics 13*, 99-115.

[11] Guckenheimer, J., & Holmes, P. (1983). Nonlinear Oscillations, Dynamic Systems, and Bifuractions of Vector Fields. *Applied Mathematical Sciences 42*, New York.

[12] Haessig Jr., D.A., & Frieland B. (1991). On the Modeling and Simulation of Friction. *Journal of Dynamic Systems, Measurement and Control 113*(3), 354-362.

[13] Hensen, R.H.A., Angelis, G.Z., Molengraft van de, M.J.G., Jager de, A.G., & Kok, J.J. (2000). Grey-box modeling of friction: An experimental case-study. to appear in the *European Journal of Control 3*.

[14] Karnopp, D. (1985). Computer Simulation of Stick-Slip Friction in Mechanical Dynamic Systems. *ASME Journal of Dynamic Systems, Measurement and Control 107*, 100-103.

[15] Leine, R.I., van Campen, D.H., de Kraker, A., & van den Steen, L. (1998). Stick-Slip Vibrations Induced by Alternate Friction Models. *Nonlinear Dynamics 16*, 41-54.

[16] Leine, R.I., van Campen, D.H., & van de Vrande, B.L. (2000). Bifurcations in Nonlinear Discontinuous Systems. *Nonlinear Dynamics*, Vol. 23, **2**, 105-164.

[17] Leine, R.I. (2000). Bifurcations in Discontinuous Mechanical Systems of Filippov Type. Ph.D. Thesis, Eindhoven University of Technology, The Netherlands.

[18] Olsson, H., & Åström, K.J. (1996). Friction generated limit cycles. In *Proc. of the 1996 IEEE Conference on Control Applications*, Dearborn, MI, 798-803.

[19] Parker, T.S., & Chua, L.O. (1989). Practical Numerical Algorithms for Chaotic Systems. New York: Springer-Verlag.

[20] Radcliffe, C.J., & Southward, S.C. (1990). A property of stick-slip friction models which promotes limit cycle generation. *Proc. 1990 American Control Conference.*, ACC, San Diego, CA, 1198-1203.